Eur. Phys. J. A (2016) **52**: 82
DOI 10.1140/epja/i2016-16082-5

THE EUROPEAN PHYSICAL JOURNAL A

Review

Experimental data on solar neutrinos*

Livia Ludhova[a]

INFN, Sezione di Milano, via Celoria 16, 20133, Milano, Italia

Received: 9 July 2015
Published online: 8 April 2016 –
Communicated by C. Broggini

Abstract. Neutrino physics continues to be a very active research field, full of opened fundamental questions reaching even beyond the Standard Model of elementary particles and towards a possible new physics. Solar neutrinos have played a fundamental historical role in the discovery of the phenomenon of neutrino oscillations and thus non-zero neutrino mass. Even today, the study of solar neutrinos provides an important insight both into the neutrino as well as into the stellar and solar physics. In this section we give an overview of the most important solar-neutrino measurements from the historical ones up to the most recent ones. We cover the results from the experiments using radio-chemic (Homestake, SAGE, GNO, GALLEX), water Cherenkov (Kamiokande, Super-Kamiokande, SNO), and the liquid-scintillator (Borexino, KamLAND) detection techniques.

1 Introduction

The Sun, our closest star is powered by nuclear reactions in which hydrogen is fused to ^{4}He. These reactions require extreme temperatures and thus they occur only in the Sun's core. It takes at the order of 10^5 years that electromagnetic radiation released in these fusion reactions reaches the Sun's surface, can escape and reach the Earth. To the contrary, neutrinos interacting only through the weak interactions, escape immediately from the place of their origin (with the speed close to that of light) and in few minutes bring to us a prove of nuclear origin of solar energy.

The energy spectrum of solar neutrinos is shown in fig. 1. Such spectra are predicted by the so-called Standard Solar Model (SSM), the stellar evolution model in which development had a pioneering role J. Bahcall [3]. The SSMs consider among several other input parameters (solar age, mass, luminosity, radiation opacity) also the chemical composition of the Sun. Different solar compositions (*e.g.*, high metallicity[1] [4] and low metallicity [5]) predict different solar-neutrino fluxes. More details about the SSM and the so-called "metallicity problem" can be found in [6].

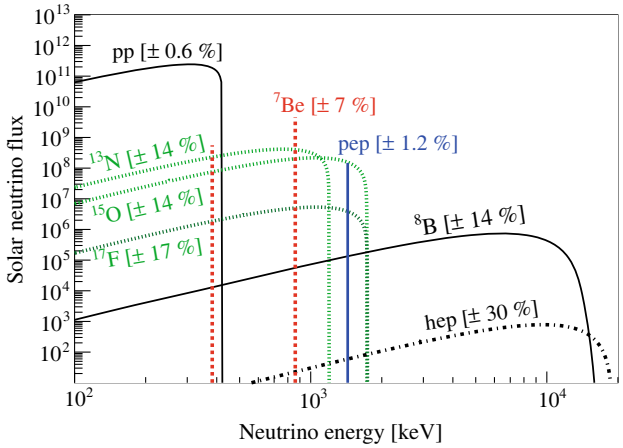

Fig. 1. Energy spectrum of solar neutrinos taken from [1]. The spectral shapes are taken from [2] while the flux normalisation from [4]. The vertical axis report the flux in cm^{-2} s^{-1} MeV^{-1} for the continuous neutrino spectra, while in cm^{-2} s^{-1} for the monochromatic lines. The numbers in parenthesis represent the theoretical uncertainties on the expected fluxes.

The SSM identifies two distinct $4p \rightarrow {}^4$He fusion processes: the so-called *pp* and the CNO cycles. The CNO cycle is thought to power mostly very massive stars, while in the Sun it is expected to produce less than 1% of its energy. The neutrinos expected to be produced in this cycle are shown in green in fig. 1 and to date there is no experimental evidence of their existence. The dominant part of the solar energy is produced in the *pp* cycle, producing the low-energy *pp* neutrinos with the energies

* Contribution to the Topical Issue "Underground nuclear astrophysics and solar neutrinos: Impact on astrophysics, solar and neutrino physics" edited by Gianpaolo Bellini, Carlo Broggini, Alessandra Guglielmetti.

[a] e-mail: livia.ludhova@mi.infn.it

[1] Metallicity = abundance of heavy elements with Z above He.

up to 420 keV, mono-energetic *pep* neutrinos (1442 keV) and ^{7}Be (862 and 384 keV) neutrinos, and a small flux of higher-energy ^{8}B neutrinos extending above 10 MeV.

The measurement of solar neutrinos lead to the discovery of the phenomenon of lepton-flavor changing neutrino oscillations. This effect was first considered by Pontecorvo [7–9], already in the 1950s, a long time before any experimental indications. The emerging hint of the so-called Solar-Neutrino Problem at the beginning of the 1970s from the first results of the pioneering chlorine experiment (whose final findings are summarised in [10]), carried out by Ray Davies in the Homestake mine, marked the experimental beginning of the neutrino oscillation saga. Consistently with Homestake results, also other experiments detecting solar neutrinos in the 1980s and 1990s (Kamiokande, GALLEX, SAGE) [11–13] have all detected fluxes significantly reduced with respect to the SSM expectations. In addition, this reduction was observed to be energy dependent. The direct evidence for neutrino flavor transformation came from the SNO experiment [14], the first able to detect neutrinos of all flavors (electron, muon, and tau) and to confirm that the total flux of neutrinos is consistent with the SSM predictions. Thus, the deficit observed in earlier experiments was due to the inefficiency to detect muon and tau neutrinos, to which the electron flavor neutrinos, originally produced in fusion reactions, are converted in the process of neutrino oscillations. The energy dependence of the probability of this conversion is explained today by the interactions between neutrinos and a dense matter inside the Sun (composed of electrons and not muons and taus), the resonance-like MSW effect [15–17]. The effect of neutrino oscillations have been then observed also on reactor neutrinos by KamLAND [18] and on atmospheric neutrinos by Super-Kamiokande [19].

As we have seen, solar neutrinos have played a fundamental historical role in the discovery of the phenomenon of neutrino oscillations and thus non-zero neutrino mass. Even today, the study of solar neutrinos provides an important insight both into the stellar and solar physics [6] as well as neutrino physics [20]. In this paper, we give an overview of the most important solar-neutrino measurements from the historical ones up to the most recent ones. The results from the radiochemical experiments (Homestake, SAGE, GNO, GALLEX) are described in sect. 2, while the water Cherenkov (Kamiokande, Super-Kamiokande, SNO), and the liquid-scintillator (Borexino, KamLAND) experiments in sects. 3 and 4, respectively.

2 Radiochemical experiments

The radiochemical detection technique was the one used in the first detection of solar neutrinos, performed by the Homestake experiment [10]. This achievement gained a Noble Prize to Ray Davis, the leader of this experiment, in 2002. The principle of the radiochemical technique, described in detail in [21], is very simple: the detection medium is a material which, upon absorption of a neutrino, is converted into a radioactive element whose decay is afterwards detected and counted. However, the real challenge of such measurements is the smallness of the signal: in about two decades of operation, Homestake and SAGE detected 860 [10] and 870 [28] decays in the targets of 615 and 13 tons, respectively.

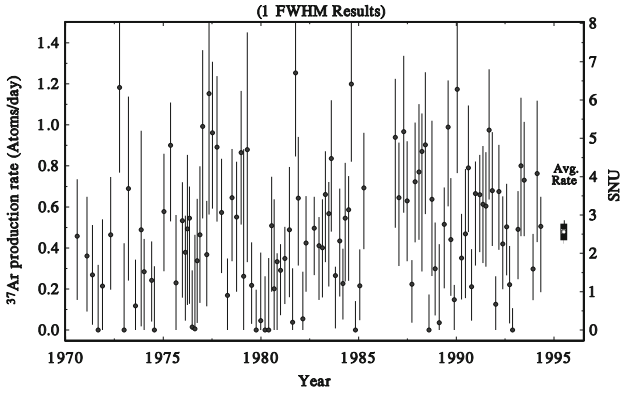

Fig. 2. Results for 108 individual extractions and thus, solar-neutrino observations, made by Homestake in two decades from the 1970s to the 1990s [10]. The shown errors are statistical only. The error shown for the cumulative result is the combination of the statistical and systematic errors in quadrature.

All radiochemical experiments are counting experiments. Thus, their result is the total interaction rate of all neutrinos above a certain energy threshold. This threshold was 814 keV for ^{37}Cl-based detection used by Homestake and 233 keV for ^{71}Ga-based detection used by GALLEX/GNO and SAGE. Homestake was measuring predominantly ^{8}B neutrinos with about 20% contribution from other sources, mainly ^{7}Be. The principal difference of these two techniques is, looking at fig. 1, that ^{71}Ga-based experiments have been detecting also the low-energy *pp* neutrinos, dominating the solar-neutrino flux. The main disadvantage, with respect to the real-time water Cherenkov and liquid-scintillator–based experiments, is that with the radiochemical technique it is not possible to disentangle the individual contribution of different spectral species to the integral signal measured above the detection threshold.

The results of the Homestake experiment [10], situated in Homestake Gold Mine, at Lead, South Dakota, are shown in fig. 2, showing the ^{37}Ar production rate (non-solar ^{37}Ar production subtracted), directly proportional to the integral solar-neutrino interaction rate (shown in the so-called Solar-Neutrino Unit (SNU)[2]), as a function of time. Homestake provided the first solar-neutrino detection in early 1970s and continued to take data until mid 1990s. Each point on the plot represents one individual ^{37}Ar extraction. The combined result of 108 extractions is a solar-neutrino–induced ^{37}Ar production rate of 2.56 ± 0.16 (stat) ± 0.16 (sys) SNU.

After the first Homestake results in the 1970s, the results of ^{71}Ga-based GALLEX/GNO and SAGE experiments came in the 1990s. The deficit of the observed solar-neutrino signal with respect to the SSM model predictions

[2] 1 Solar-Neutrino Unit (SNU) = 1 interaction per 10^{36} target nuclei per second.

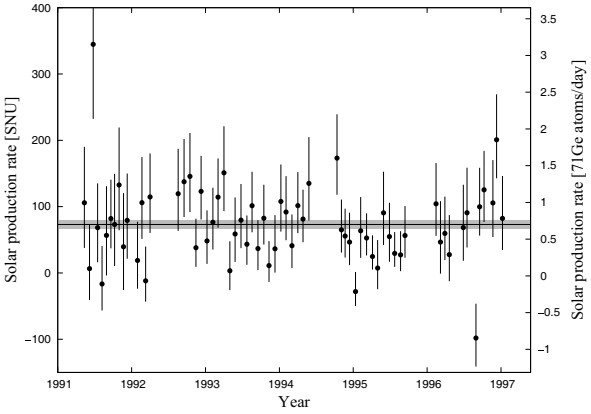

Fig. 3. GALLEX results [25] based on 65 solar runs taken in the years 1991–1997. The error bars are $\pm 1\sigma$ statistical.

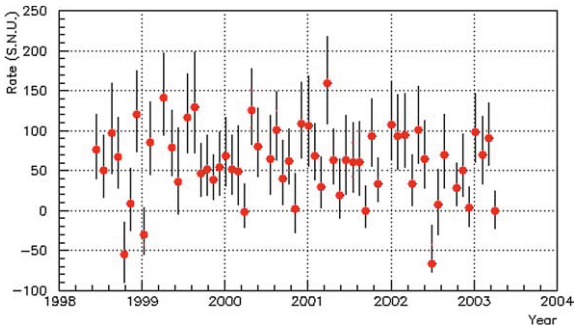

Fig. 4. GNO results [26] based on 58 solar exposure runs taken in the years 1998–2003.

was confirmed. The fraction of the observed signal (with respect to the SSM) was found to be energy dependent, about 40% for the solar-neutrino flux above 814 keV and about 67–69% for the solar-neutrino flux above 233 keV.

The GALLEX and GNO experiments, both placed in the Laboratori Nazionali del Gran Sasso underground laboratory in Italy, have been taking data in the years 1991–1997 and 1998–2003, respectively. GALLEX have provided its results in 4 different phases [11,22–24]. A new reanalysis [25] of all GALLEX data have been published in 2010. A better calibration and an advanced analysis technique yielded an overall result of $73.4^{+7.1}_{-7.3}$ SNU, about 5.3% lower with respect to the original evaluations. Figure 3 shows the stability of the observed signal, shown individually for all 65 extractions.

The GNO experiment, a GALLEX successor, has provided its results based on 58 solar runs taken in three phases, as they are shown in fig. 4. A global GNO result [26] is $62.9^{5.5}_{5.3}$ (stat) ± 2.5 (sys) SNU, while a global GALLEX + GNO result is 69.3 ± 5.5 SNU, including both statistical and systematic errors.

The Russian-American experiment SAGE, placed in the Baksan Neutrino Observatory in Caucasus region of Russia, began to measure the solar-neutrino capture rate with a target of gallium metal in December 1989. The first results have been published in 1999 [12] and 2002 [27], while the results of 2002–2007 data taking period in

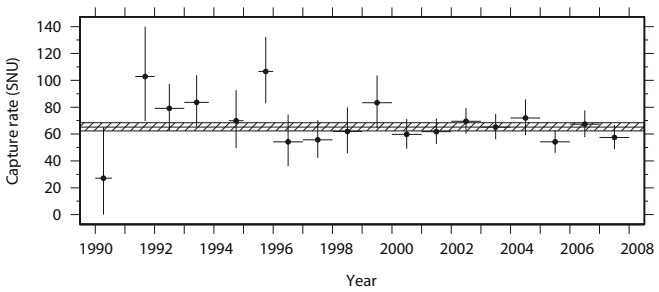

Fig. 5. SAGE results for the years 1990–2007 [28]. Shaded band is the combined best fit and its uncertainty for all years. Vertical error bars are statistical with 68% confidence.

2009 [28]. Assuming the solar-neutrino production rate was constant during the period of data collection, combined analysis of all 168 extractions taken since 1990 to 2007 gives a capture rate of solar neutrinos with energy more than 233 keV of $65.4^{+3.1}_{-3.0}$ (stat) $^{+2.6}_{-2.8}$ (sys) SNU. Figure 5 shows the stability of SAGE results in 1-year bins.

GALLEX and SAGE experiments have been calibrated with reactor-produced neutrino ^{51}Cr source and SAGE also with ^{27}Ar neutrino source [29]. For all these calibrations a significant 10–20% deficit with respect to the expectations have been observed. Possible explanations range from over-estimation of the cross section for neutrino capture by the two lowest-lying excited states in ^{71}Ge to hypothetical sterile neutrinos. If these questionable cross sections are zero, then the SSM including neutrino oscillations predicts a total capture rate in Ga in the range of 63–66 SNU with an uncertainty of about 4%, in a good agreement the experiment.

3 Water Cherenkov experiments

Water-based Cherenkov detection technique, described in detail in [30], is widely used in real-time detection of ^{8}B solar and atmospheric neutrinos. The Cherenkov radiation is produced in a material with refractive index n by a charged particle if its velocity is greater than the local phase velocity of the light. The resulting light wavefront is conical and this brings the main advantage of this technique: directionality measurement. In case of solar neutrinos, this means a possibility to reduce the background by selecting only the events with the direction pointing from the Sun. The main drawback instead is a relatively high energy threshold of these measurements (3–5 MeV, thus only ^{8}B solar neutrinos are detected, see fig. 1) and a relatively low light yield.

Kamiokande experiment, placed in the Kamioka mine in Japan (and today upgraded to Super-Kamiokande detector), was the first to perform the real-time detection of solar neutrinos [13], ^{8}B neutrinos above 9.3 MeV energy threshold. This was a fundamental result confirming the deficit of the measured neutrino flux with respect to the SSM prediction, observed for the first time in the 1970s by the ^{37}Cl-based radiochemical Homestake experiment.

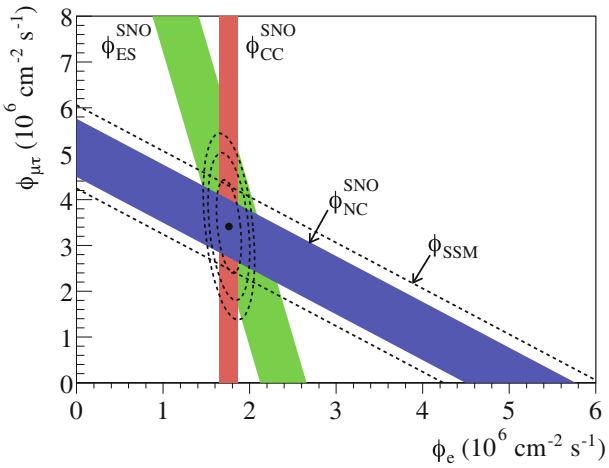

Fig. 6. Flux of ^{8}B solar neutrinos which are μ or τ flavor *vs.* flux of electron neutrinos deduced from the three neutrino reactions in SNO [31]. The diagonal bands show the total ^{8}B flux as predicted by the Standard Solar Model [32] (dashed lines) and that measured with the NC reaction in SNO (solid band). The intercepts of these bands with the axes represent the $\pm 1\sigma$ errors. The bands intersect at the fit values for Φ_e and $\Phi_{\mu\tau}$, indicating that the combined flux results are consistent with neutrino flavor transformation assuming no distortion in the ^{8}B neutrino energy spectrum.

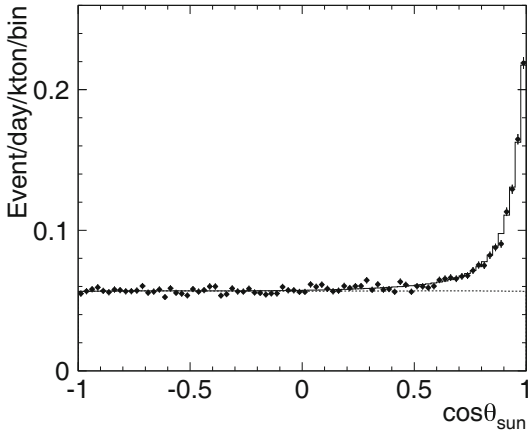

Fig. 7. The angular distribution of the solar-neutrino final sample events measured by Super-Kamiokande [40]. The dotted line seen under the peak in the solar direction represents background contributions.

After 30 years long saga of *solar-neutrino problem*, it was a heavy-water–based Cherenkov detector SNO, placed in the Sudbury mine in Canada, which came with a solution [14] in 2002: a direct evidence for neutrino flavor transformation. This result is demonstrated in fig. 6 taken from an updated analysis [31] from 2007. This extraordinary result was achieved because SNO was able to detect neutrinos with three types of interactions, represented by three coloured bands in fig. 6. Each interaction had different sensitivities to different neutrino flavors. Thanks to heavy-water deployment, SNO was the first experiment to be able to detect neutrinos via neutral-current interactions (blue band), having the same cross-section for all their flavors. Charged-current interactions (employed also in radiochemical experiments) are sensitive only to electron flavor neutrinos and so the red band in fig. 6 is parallel to the y-axis showing the measured flux of μ and τ neutrinos. Elastic scattering (used in non–heavy-water Cherenkov detection) can proceed via charge current (electron flavor only) and neutral current (all flavors) interactions. This means, the total elastic-scattering cross section has different value for different flavors and is predominately sensitive to electron flavor: the green band in fig. 6 is not completely vertical as the red band, bad has a different slope with respect to the blue band. The power of the SNO result is that all three bands do cross in the same region and that the total observed neutrino flux of all flavors is consistent with the SSM predictions.

A Low-Energy-Threshold Analysis (LETA) of Phase I and Phase II SNO data [33] succeeded in lowering the effective electron kinetic energy threshold from 5 MeV to 3.5 MeV. The SNO Phase III [34], lasting from 2004 to 2006, was characterised by an improved sensitivity to neutral-current interactions thanks to the implementation of an array of Neutral-Current Detectors, the lowest-radioactivity large array of proportional counters ever produced. This array consisted of 36 strings of proportional counters filled with a mixture of ^{3}He and CF_4 gas capable of detecting the neutrons liberated by the neutrino-deuteron neutral current reaction in heavy water and four strings filled with a mixture of ^{4}He and CF_4 gas for background measurements. Recently in 2013, an updated Phase III analysis with an improved background rejection based on particle identification from proportional counters, combined with Phase I and II results [35] resulted in a new evaluation of the total flux of active flavuors of ^{8}B solar neutrino as $(5.25 \pm 0.16\ (\text{stat.})\ ^{+0.11}_{-0.13}\ (\text{sys.}))$ $\times 10^6\,\text{cm}^{-2}\text{s}^{-1}$. After the end of SNO data taking, the heavy water was replaced with liquid scintillator. The SNO+ experiment, a successor of SNO, has as its main aim the measurement of neutrino-less double beta decay, but expects to continue also with the solar-neutrino program.

After the first Kamiokande detection of ^{8}B solar neutrinos 1989 [13], this experiment provided also a clear directional measurement [36] proving the solar origin of the observed signal.

The Super-Kamiokande experiment started in 1996, being a successor of Kamiokande. It obtained its first results after the first 300 days of measurement [37] with an energy threshold of 6.5 MeV. The experiment provided the results of its Phase I [38] in 2006, Phase II [39] in 2006, and most recently in 2011 for its Phase III [40] with 5 MeV threshold. A very clear demonstration of solar origin of measured neutrinos is shown in fig. 7, showing the signal angular distribution as measured during the Phase III. Based on the same Phase III data, fig. 8 shows the ratio of observed and expected energy spectra above 5 MeV. Based on a recent analyses [41], fig. 9 shows the measured electron-neutrino survival probability for ^{8}B solar neutrinos in energy range 3–20 MeV for

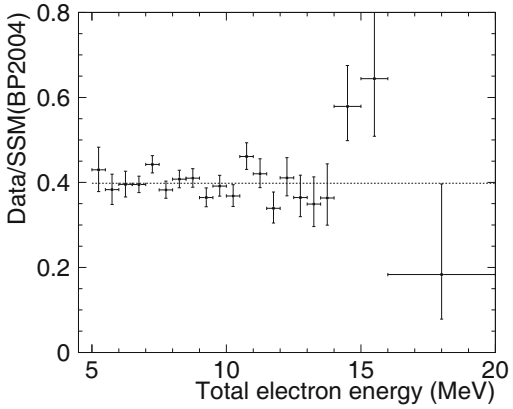

Fig. 8. Ratio of observed and expected energy spectra measured by Super-Kamiokande [40]. The dashed line represents the SK-III average.

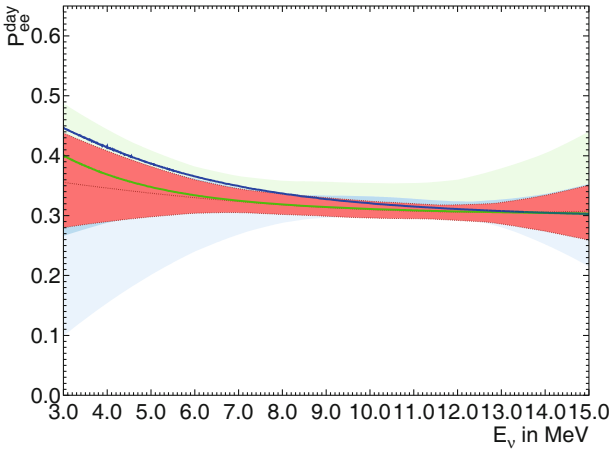

Fig. 9. Electron-neutrino survival probability as a function of energy as measured on ^{8}B solar neutrinos above 3 MeV by SNO and Super-Kamiokande collaborations [41] as measured during the day (without terrestrial matter effects). The blue and green areas are 1σ bands for SNO [35] and Super-Kamiokande, while the red one is a combined analysis of these two results. The thick solid lines are LMA-MSW predictions using the oscillation parameters from the global fit of all solar + KamLAND data (blue, $\sin^2\theta_{12} = 0.308$ and $\Delta m^2_{12} = 7.50 \times 10^{-5}\,\mathrm{eV}^2$) and solar only (green, $\sin^2\theta_{12} = 0.311$ and $\Delta m^2_{12} = 4.85 \times 10^{-5}\,\mathrm{eV}^2$).

combined Super-Kamiokande + SNO [35] data, compared to individual results of each experiment.

Very recently in 2014, Super-Kamiokande provided the first indication of terrestrial matter effects on solar-neutrino oscillation based on data from Phases I-IV [42]. They report an indication that the elastic scattering rate of solar ^{8}B neutrinos with electrons in the detector is larger when the neutrinos pass through the Earth during nighttime. They determine the day-night asymmetry, defined as the difference of the average day rate and average night rate divided by the average of those two rates, to be $(-3.2 \pm 1.1\ (\mathrm{stat})\ \pm 0.5\ (\mathrm{sys}))\%$, which deviates from zero by 2.7σ. Since the elastic scattering process is

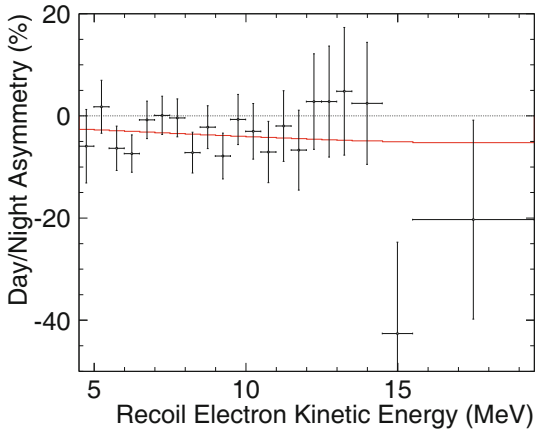

Fig. 10. Super-Kamiokande day-night amplitude fit as a function of recoil electron kinetic energy [42], shown as the measured amplitude times the expected day-night asymmetry, for oscillation parameters chosen by the SK best fit. The error bars shown are statistical uncertainties only and the expected dependence is shown in red.

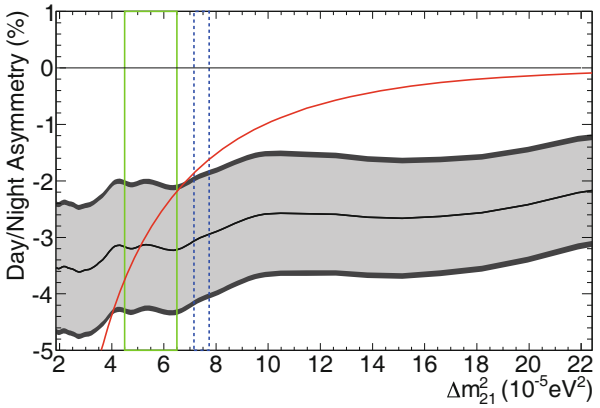

Fig. 11. Dependence of the measured day-night asymmetry (fitted day-night amplitude times the expected day-night asymmetry (red)) on Δm^2_{12} for $\sin^2\theta_{12} = 0.314$ and $\sin^2\theta_{13} = 0.015$ [42]. The 1σ statistical (systematic) uncertainties are given by the light (dark) grey bands, respectively. The vertical lines indicate the 1σ allowed ranges from the solar global fit (solid green) and the KamLAND experiment (dashed blue).

mostly sensitive to electron flavor solar neutrinos, a non-zero day-night asymmetry implies that the flavor oscillations of solar neutrinos are affected by the presence of matter within the neutrinos' flight path. Figure 10 shows the observed energy dependence of the observed asymmetry in 5–20 MeV energy range. Dependence of the measured day-night asymmetry on Δm^2_{12} is demonstrated in fig. 11.

4 Liquid-scintillator experiments

A successful implementation of the liquid-scintillator detection technique, described in detail in [43], was a breakthrough for a low-energy solar-neutrino physics. Only with this technique it was possible to perform real-time

spectroscopic measurements of all species of solar-neutrino spectrum below 1 MeV.

The main advantage of this method is the high light yield and thus a good energy resolution and, in principle, a possibility of a low-energy threshold. However, to the contrary of water Cherenkov detection, the information about the direction of the incident particle is lost. This in turn means that the background suppression based on the angular distribution with respect to the Sun is not possible. It took several years to develop the methods of purification of the scintillator and of surface treatment of other construction materials, until Borexino detector, placed in the underground Laboratori Nazionali del Gran Sasso in central Italy, came to a successful operation in May 2007.

The original goal of the Borexino experiment was the detection of mono-energetic 862 keV ^{7}Be solar neutrinos, with the expected interaction rate of about 50 events/day/100 ton. In order to be able to see such a faint signal, the required level of radio-purity of liquid scintillator is about 9–10 orders of magnitude lower than the natural ambient radioactivity. With the techniques described in [44], Borexino exceeded this goal and reached unprecedented levels of radio-purity. Thanks to this achievement, the first detection of ^{7}Be solar neutrinos [45] has been possible with the first 192 days of collected data.

Soon after, the first result was followed by the second measurement [46] and then, after an extensive calibration of the detector with radioactive sources, by a 5% precision measurement [47] in 2011. Borexino performed the first detection of *pep* neutrinos [48] in 2012. The same analysis provided also to-date best limit on the CNO solar-neutrino flux. These low-energy solar-neutrino results of Borexino Phase I (2007–2010) have been described in detail in [49], considering updated neutrino oscillation parameters from [50].

The experimental signature of ^{7}Be neutrino interactions in Borexino is a Compton-like shoulder at 660 keV, clearly visible at the energy spectra shown in fig. 12. Fits to the spectrum of observed event energies are used to distinguish between this neutrino scattering feature and the backgrounds from radioactive decays. Figure 12 shows in different colours various species used in the fit performed by two independent methods giving consistent results. The interaction rate of the 862 keV ^{7}Be solar neutrinos was determined to be 46 ± 1.5 (stat) $^{+1.5}_{-1.6}$ (sys) cpd (see footnote[3])/100 ton. If the detected neutrinos are assumed to be purely ν_e, this corresponds to neutrino flux of $(2.79 \pm 0.13) \times 10^{9}\,\mathrm{cm^{-2}\,s^{-1}}$. Considering the 3-flavor neutrino oscillations, the equivalent flux is $(4.43 \pm 0.22) \times 10^{9}\,\mathrm{cm^{-2}\,s^{-1}}$. The electron neutrino survival probability turns out to be $0,1 \pm 0.07$. The day-night asymmetry of ^{7}Be solar-neutrino signal was excluded [51] at the level of $A_{dn} = 0.001 \pm 0.012$ (stat) ± 0.007 (sys), in agreement with the prediction of MSW-LMA solution for neutrino oscillations. This result, for the first time, completely disfavoured the LOW solution (8.5σ) without the use of reactor antineutrino data, as it is demonstrated in fig. 13.

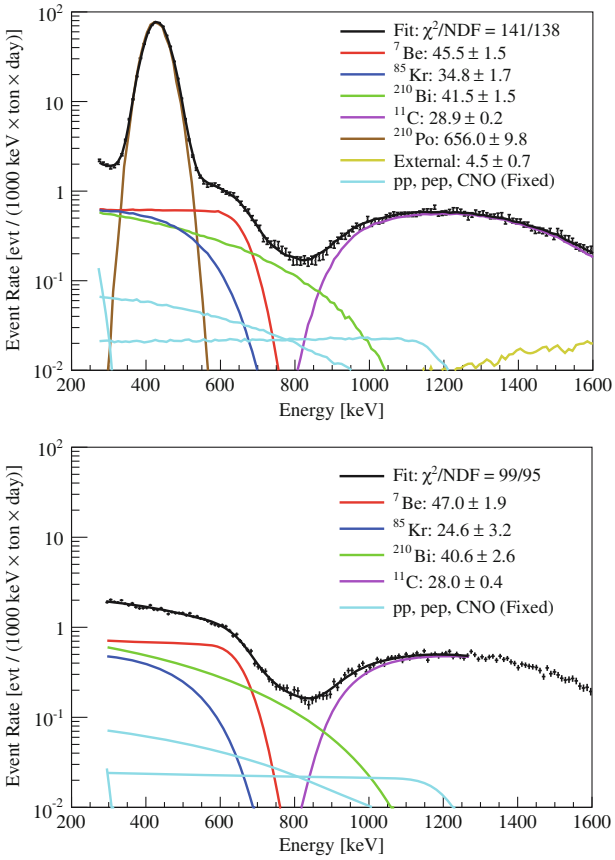

Fig. 12. Examples of the fits of the Borexino energy spectrum in order to extract the ^{7}Be solar-neutrino interaction rate with 5% precision [47]. The fit results in the legends have units [cpd/100 ton] and give total rates independent of the fit energy window. The upper plot shows a Monte-Carlo–based fit in the energy region 270–1600 keV. The bottom plot demonstrates analytical approach and a fit over the 290–1270 keV energy range after the statistical α-subtraction of mostly ^{210}Po events.

Figure 14 shows the Borexino energy spectrum used to extract the first *pep* solar-neutrino measurement and the current best limit on the CNO solar-neutrino flux [48]. The necessary sensitivity was achieved by adopting novel techniques for the rejection of $^{11}\mathrm{C}(e^{+})$ cosmogenic background dominating the 1–2 MeV energy region. The final result was obtained by a multivariate simultaneous fit of the energy spectra, radial, and pulse-shape PS-BDT parameter (optimised to distinguish e^{+} and e^{-}/γ signals) distributions. The measured *pep* interaction rate is 3.1 ± 0.6 (stat) ± 0.3 (sys) cpd/100 ton and the corresponding ν_e-equivalent flux is $(1.0 \pm 0.22) \times 10^{8}\,\mathrm{cm^{-2}\,s^{-1}}$. Considering the 3-flavor neutrino oscillations, the equivalent flux is $(1.63 \pm 0.35) \times 10^{8}\,\mathrm{cm^{-2}\,s^{-1}}$. The CNO interaction rate is constrained to < 7.9 cpd/100 ton at 95% CL and the CNO solar-neutrino flux to $< 7.7 \times 10^{8}\,\mathrm{cm^{-2}\,s^{-1}}$.

Borexino reported also the measurement of $\nu - e$ elastic scattering from ^{8}B solar neutrinos with 3 MeV energy threshold [52]. The observed interaction rate is

[3] cpd = counts/day.

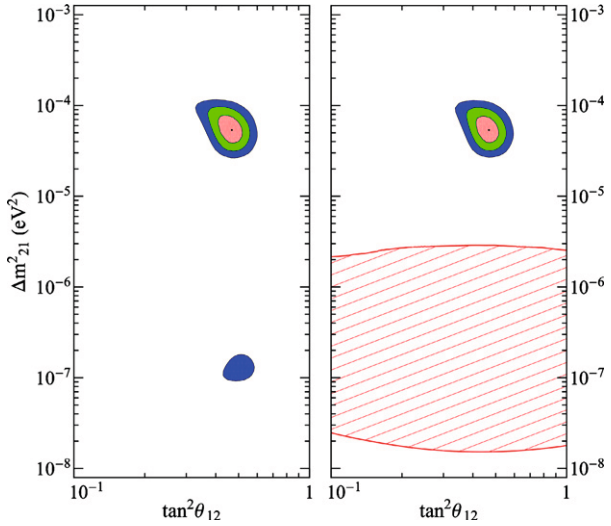

Fig. 13. The LOW region of neutrino oscillation parameters was allowed at the 99.73% CL by the solar-neutrino only global fit before the Borexino exclusion of a day-night effect for ^{7}Be neutrinos at 1% level [51]. This allowed LOW region with $\Delta m^2 \sim 10^{-7}$ is shown in blue at the left part of the plot. The hatched red region in the right panel shows the region of oscillation parameters excluded by this Borexino day-night measurement.

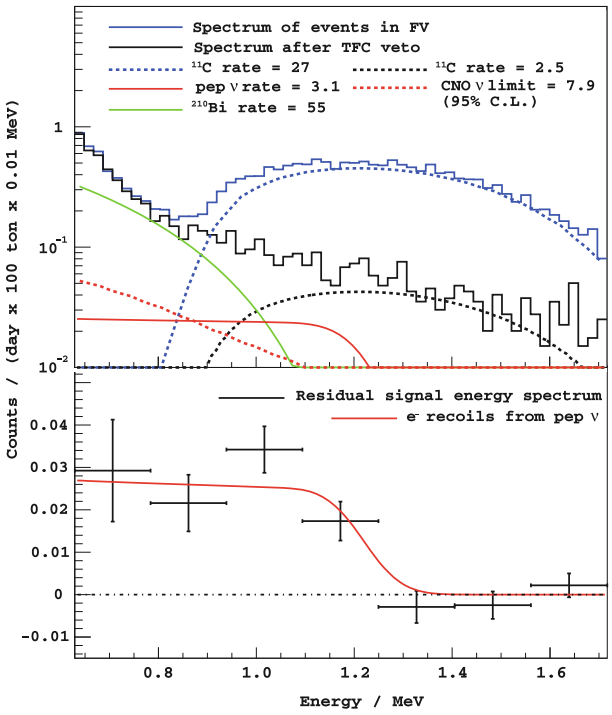

Fig. 14. Borexino energy spectrum to extract the first *pep* solar-neutrino measurement and the current best limit on the CNO solar-neutrino flux [48]. Top: energy spectra before (blue solid line) and after (black solid line) the TFC veto is applied. The dashed blue and black lines show the corresponding ^{11}C rates. The next largest background, ^{210}Bi (green), and the e^- recoil spectra of the best estimate of the *pep*-neutrino rate (solid red) and of the upper limit of the CNO-neutrino (dashed red) rate are shown for reference. Rate values in the legend are integrated over all energies and are quoted in units of [cpd/100 ton]. Bottom: residual energy spectrum after best-fit rates of all considered backgrounds are subtracted with the *pep*-neutrino best fit shown for comparison.

0.22 ± 0.04 (stat) ± 0.01 (sys) cpd/100 ton, which under the assumption of no-oscillations corresponds to flu $2.4 \pm 0.4 \pm 0.1 \times 10^6\,\mathrm{cm}^{-2}\,\mathrm{s}^{-1}$, in good agreement with measurements from SNO and Super-Kamiokande. Assuming the ^{8}B neutrino flux predicted by the high-metallicity standard solar model, the average ^{8}B-ν_e survival probability above 3 MeV is measured to be 0.29 ± 0.10. The measured ^{8}B energy spectrum is shown in fig. 15.

Borexino performed the first real-time detection of *pp*-neutrinos [53] which, according to Physics World, was listed among the Top 10 Physics Breakthroughs of 2014. The main difficulty in measuring this low-energy solar neutrinos is that their spectrum (264 keV end-point) is overburden under the ^{14}C-beta spectrum (156 keV Q-value). In spite of a tiny isotopic fraction of ^{14}C in the Borexino scintillator ($^{14}\mathrm{C}/^{12}\mathrm{C} < 2.7310218$), ^{14}C-$\beta$-decay is responsible for most of the detector triggering rate ($\sim$ 30 counts/second). A correlated difficulty comes from the so-called ^{14}C pile-up, *e.g.* when the two uncorrelated events occurring in a short time window are measured as a single event. The final fit of the energy spectrum between 165 and 590 keV is shown in fig. 16. The measured solar *pp*-neutrino interaction rate is 144 ± 13 (stat) ± 10 (sys) cpd/100 ton and the corresponding electron neutrino survival probability is 0.64 ± 0.12.

Figure 17 confronts the LMA-MSW prediction of the electron neutrino survival probability for solar neutrinos with the data points based on Borexino measurements: *pp*, *pep*, ^{7}Be, and ^{8}B solar neutrinos. After the spectroscopic measurements of low-energy solar neutrinos, the LMA-MSW is being pinned down with increased precision. At the same time, the data points are putting strong limits

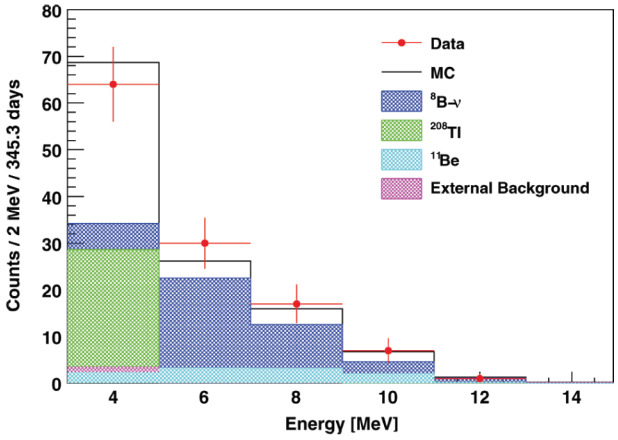

Fig. 15. Borexino energy spectrum (red dots) after selection cuts above 3 MeV, used to extract the ^{8}B neutrino rate [52], compared to Monte Carlo simulations (black line).

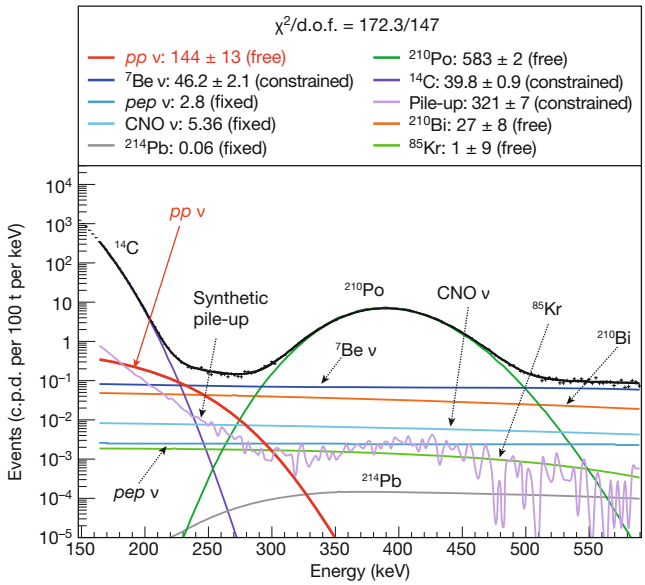

Fig. 16. Borexino fit of the energy spectrum between 165 and 590 keV in order to extract the *pp*-neutrino rate [53]. The best-fit *pp*-neutrino component is shown in red. The values of the rates of all spectral components (in [cpd/100 ton]) are in the insert above the figure.

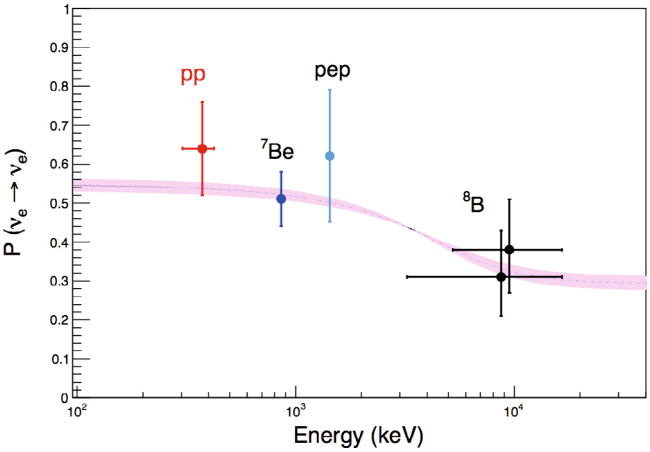

Fig. 17. Survival probability of electron-neutrinos produced by the different nuclear reactions in the Sun [53]. The violet band corresponds to the 1σ prediction of the MSW-LMA solution [50]. It is calculated for the ^{8}B solar neutrinos, considering their production region in the Sun which represents the other components well. All data points are measured by Borexino, the vertical error bars represent the 1σ interval; the horizontal uncertainty shows the neutrino energy range used in the measurement.

on the predictions of theories of non-standard neutrino interactions. For more details, consult [54–57].

KamLAND experiment, 1 kton liquid-scintillator detector placed in Kamioka mine in Japan, was originally constructed to measure reactor antineutrinos. Based on these measurements, KamLAND provided the first evidence of neutrino oscillation pattern [18] and the strongest constraint on the value of Δm^2_{12} parameter [58]. In liquid scintillators, antineutrinos are detected via inverse-β

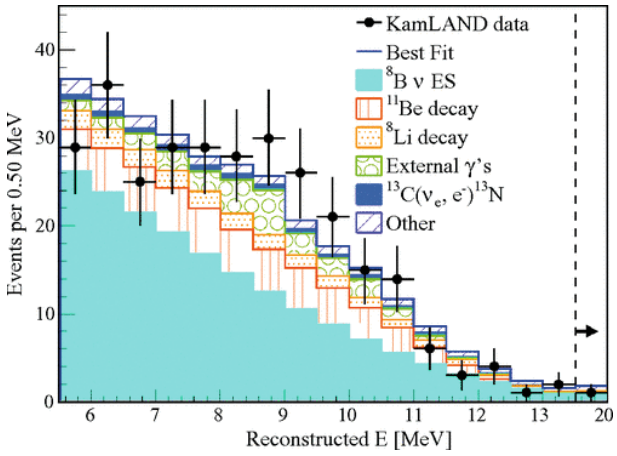

Fig. 18. Energy spectrum of ^{8}B candidates with the best-fit spectrum and background components from the unbinned energy and rate analysis [59].

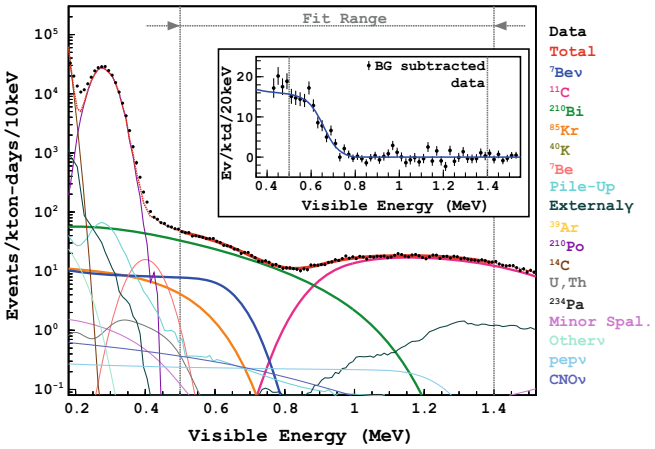

Fig. 19. KamLAND rank-1 energy spectrum (black dots) used in the simultaneous fit to all rank's spectra in order to extract the ^{7}Be solar-neutrino interaction rate [60]. The fit range is 500–1400 keV. The inset shows the background subtracted spectrum.

decay interaction $\bar{\nu}_e + p \rightarrow e^+ + n$, yielding a golden delayed coincidence tag (prompt e^+ signal and the delayed γ-signal from the neutron capture) strongly suppressing other backgrounds. KamLAND thus did not require to reach the radio-purity of Borexino, having its primary aim the measurement of singles from electrons scattered of solar neutrinos, indistinguishable from other backgrounds. In spite of that, KamLAND succeeded in measuring the solar neutrinos through the elastic scattering off electrons. The background-subtracted electron recoil rate above a 5.5 MeV analysis threshold due to ^{8}B solar neutrinos (see fig. 18) is 1.49 ± 0.14 (stat) ± 0.17 (sys) cpd/kton [59]. Interpreted as due to a pure electron flavor flux with a ^{8}B neutrino spectrum, this corresponds to a spectrum integrated flux of 2.7 ± 0.26 (stat) ± 0.32 (sys) $\times 10^6\,\mathrm{cm}^{-2}\,\mathrm{s}^{-1}$. KamLAND has measured also ^{7}Be solar neutrinos [60]. The final rank-1 energy spectrum[4]

[4] The analysis is performed in different volume partitions; to each is assigned a rank, based on the average estimated

and the fit are shown in fig. 19. The observed rate of 862 keV ^{7}Be solar neutrinos is 582 ± 90 cpd/kton. Assuming a pure electron flavor, this corresponds to neutrino flux of $(3.26 \pm 0.50) \times 10^{9}\,\mathrm{cm}^{-2}\,\mathrm{s}^{-1}$. Considering the 3-flavor neutrino oscillations, the equivalent flux is $(5.82 \pm 0.98) \times 10^{9}\,\mathrm{cm}^{-2}\,\mathrm{s}^{-1}$. The derived electron neutrino survival probability is 0.66 ± 0.14.

5 Conclusions and outlook

The study of solar neutrinos has proven to be a source of important discoveries and fundamental observations. In this section, we gave an overview of the most important solar-neutrino measurements from the historical ones up to the most recent ones, including results from the radiochemical (Homestake, SAGE, GNO, GALLEX), water Cherenkov (Kamiokande, Super-Kamiokande, SNO), and the liquid-scintillator (Borexino, KamLAND) experiments. The impact of these measurements on the current understanding of neutrino physics, the phenomenon of neutrino oscillations, and possible non-standard neutrino interactions is vastly discussed in [20], while the insight they bring to the solar and stellar physics is discussed in [6].

Even today, the solar-neutrino physics is an active field. Borexino experiment has entered in its Phase II in 2012, after an extensive purification campaign in which ^{85}Kr was almost entirely removed, while the level of ^{210}Bi was lowered by about of factor 3. The main scientific goal is a tentative to perform the first observation of CNO neutrino flux. The new extensive calibration of the detector with radioactive sources is planned for the second half of 2015. Measurements of ^{7}Be and *pep* solar neutrinos with improved precision are also expected. In 2016, a strong ^{144}Ce - ^{144}Pr antineutrino source will be placed below the Borexino detector. This new project, called SOX [61], has its primal aim to test the hypothesis of the existence of eV mass sterile neutrinos.

Super-Kamiokande has so far observed about ~ 7000 solar-neutrino interactions in ~ 4500 days, by far the largest sample of solar neutrinos and continues to take data. In 2014 this experiment started to take data with ~ 2.5 MeV threshold with 100% trigger efficiency. Thus, the new results based on this lower-energy solar-neutrino data are expected in near future. The lowering of threshold is of prime importance for testing the transition region of the electron neutrino survival probability.

SNO+ is a successor of the SNO project, having its main aim the measurement of neutrino-less double beta decay using ^{130}Te loaded liquid scintillator [62]. Depending on the final level of radio-purity, 1 kton SNO+ has a potential for high-precision solar-neutrino measurements. Thanks to a high level of shielding against cosmogenic background (6080 m.w.e), SNO+ is particularly suited for measurements of *pep* and CNO neutrinos.

JUNO [63] is a project of 20 kton liquid-scintillator detector in Jiangmen, China, scheduled to start taking data in 2020. The main goal of this project is determination of the neutrino mass hierarchy. Under a condition of high level of achieved radio-purity, thanks to the detector large size and an excellent energy resolution (3% at 1 MeV), JUNO has also a strong potential in measurement of solar neutrinos.

References

1. Borexino Collaboration (G. Bellini *et al.*), Phys. Rev. D **89**, 112007 (2014).
2. J. Bahcall, home page: `http://www.sns.ias.edu/~jnb/SNdata/`.
3. J. Bahcall, Sci. Am. **221**, 1, 28 (1969).
4. A. Serenelli, W.C. Haxton, C. Pena-Garay, Astrophys. J. **743**, 24 (2011).
5. M. Asplund *et al.*, Astrophys. J. Lett. **705**, L123 (2009).
6. A. Serenelli, Eur. Phys. J. A **52**, 78 (2016) contribution to this Topical Issue.
7. B. Pontecorvo, Sov. Phys. JETP **6**, 429 (1957).
8. B. Pontecorvo, J. Exp. Theor. Phys. **33**, 549 (1957).
9. B. Pontecorvo, J. Exp. Theor. Phys. **34**, 247 (1958).
10. Homestake Collaboration (B.T. Cleveland *et al.*), Astrophys. J. **496**, 505 (1998).
11. GALLEX Collaboration (P. Anselmann *et al.*), Phys. Lett. B **285**, 376 (1992).
12. SAGE Collaboration (J.N. Abdurashitov *et al.*), Phys. Rev. C **60**, 055801 (1999).
13. Kamiokande Collaboration (K. Hirata *et al.*), Phys. Rev. Lett. **63**, 16 (1989).
14. SNO Collaboration (Q.R. Amhad *et al.*), Phys. Rev. Lett. **89**, 011301 (2002).
15. L. Wolfenstein, Phys. Rev. D **17**, 2369-2374 (1978).
16. S.P. Mikheev, A.Y. Smirnov, Sov. J. Nucl. Phys. **42**, 913 (1985).
17. S.P. Mikheev, A.Y. Smirnov, Nuovo Cimento C **9**, 17 (1986).
18. KamLAND Collaboration (K. Eguchi *et al.*), Phys. Rev. Lett. **90**, 021802 (2003).
19. Super-Kamiokande Collaboration (Y. Ashie *et al.*), Phys. Rev. Lett. **93**, 101801 (2004).
20. M. Maltoni, A.Y. Smirnov, *Solar neutrinos and neutrino physics*, contribution to this Topical Issue.
21. C.M. Cattadori, L. Pandola, *Experimental and analysis methods in radiochemical experiments*, contribution to this Topical Issue.
22. GALLEX Collaboration (P. Anselman *et al.*), Phys. Lett. B **357**, 237 (1995) **361**, 235(E) (1996).
23. GALLEX Collaboration (W. Hampel *et al.*), Phys. Lett. B **388**, 384 (1996).
24. GALLEX Collaboration (W. Hampel *et al.*), Phys. Lett. B **447**, 127 (1999).
25. F. Kaether *et al.*, Phys. Lett. B **685**, 47 (2010).
26. GNO Collaboration (M. Altmann *et al.*), Phys. Lett. B **616**, 174 (2005).
27. SAGE Collaboration (J.N. Abdurashitov *et al.*), Zh. Eksp. Teor. Fiz. **122**, 211 (2002) (J. Exp. Theor. Phys. **95**, 181 (2002)).
28. SAGE Collaboration (J.N. Abdurashitov *et al.*), Phys. Rev. C **80**, 015807 (2009).

[210]Bi contamination in the neighbouring partitions; rank one corresponds to the lowest ^{210}Bi contamination.

29. B. Caccianiga, A.C. Re, Eur. Phys. J. A **52**, 80 (2016) contribution to this Topical Issue.
30. Y. Koshio, *Data Analysis in solar neutrinos by Water Cherenkov detectors*, contribution to this Topical Issue.
31. SNO Collaboration (B. Aharmin *et al.*), Phys. Rev. C 87 **75**, 045502 (2007).
32. J.N. Bahcall, M. Pinsonneault, S. Basu, Astrophys. J. **555**, 990 (2001).
33. SNO Collaboration (B. Aharmim *et al.*), Phys. Rev. C **81**, 055504 (2010).
34. SNO Collaboration (B. Aharmim *et al.*), Phys. Rev. C **87**, 015502 (2013).
35. SNO Collaboration (B. Aharmin *et al.*), Phys. Rev. C **88**, 025501 (2013).
36. Kamiokande Collaboration (K.S. Hirata *et al.*), Phys. Rev. D **44**, 2241 (1991).
37. Super-Kamiokande Collaboration (Y. Fukuda *et al.*), Phys. Rev. Lett. **81**, 1158 (1998).
38. Super-Kamiokande Collaboration (J. Hosaka *et al.*), Phys. Rev. D **73**, 112001 (2006).
39. Super-Kamiokande Collaboration (J.P. Cravens *et al.*), Phys. Rev. D **78**, 032002 (2008).
40. Super-Kamiokande Collaboration (K. Abe *et al.*), Phys. Rev. D **83**, 052010 (2011).
41. Super-Kamiokande Collaboration (Y. Koshio *et al.*), to be published in the *Proceedings of the XXVI International Conference on Neutrino Physics and Astrophysics, 2014, Boston*.
42. Super-Kamiokande Collaboration (A. Renshaw *et al.*), Phys. Rev. Lett. **112**, 091805 (2014).
43. G. Testera, *Data analysis in solar neutrinos liquid scintillator detectors*, contribution to this Topical Issue.
44. J.B. Benziger, F.P. Calaprice, Eur. Phys. J. A **52**, 81 (2016) contribution to this Topical Issue.
45. Borexino Collaboration (G. Bellini *et al.*), Phys. Rev. Lett. **101**, 091302 (2008).
46. Borexino Collaboration (G. Bellini *et al.*), Phys. Lett. B **658**, 101 (2008).
47. Borexino Collaboration (G. Bellini *et al.*), Phys. Rev. Lett. **107**, 141302 (2011).
48. Borexino Collaboration (G. Bellini *et al.*), Phys. Rev. Lett. **108**, 051302 (2012).
49. Borexino Collaboration (G. Bellini *et al.*), Phys. Rev. D **89**, 112007 (2014).
50. Particle Data Group (J. Beringer *et al.*), Phys. Rev. D **86**, 010001 (2012) and 2013 partial update for the 2014 edition.
51. Borexino Collaboration (G. Bellini *et al.*), Phys. Lett. B **70**, 22 (2012).
52. Borexino Collaboration (G. Bellini *et al.*), Phys. Rev. D **82**, 033006 (2010).
53. Borexino Collaboration (G. Bellini *et al.*), Nature **512**, 383 (2014).
54. A. Friedland, C. Lunardini, C. Peña-Garay, Phys. Lett. B **594**, 347 (2004).
55. S. Davidson, C. Peña-Garay, N. Rius, A. Santamaria, JHEP **03**, 011 (2003).
56. P.C. de Holanda, A.Yu. Smirnov, Phys. Rev. D **69**, 113002 (2004).
57. A. Palazzo, J.W.F. Valle, Phys. Rev. D **80**, 091301 (2009).
58. KamLAND Collaboration (S. Abe *et al.*), Phys. Rev. Lett. **100**, 221803 (2008).
59. KamLAND Collaboration (S. Abe *et al.*), Phys. Rev. C **84**, 035804 (2011).
60. KamLAND Collaboration (A. Gando *et al.*), arXiv:1405.6190 (2014).
61. Borexino Collaboration (G. Bellini *et al.*), JHEP **08**, 038 (2013).
62. SNO+ Collaboration (S. Biller *et al.*), arXiv:1405.3401 (2014).
63. `http://english.ihep.cas.cn/rs/fs/juno0815/`.